

# All-Small-Molecule Organic Solar Cells with Efficiency Approaching 16% and FF over 80%

Lingxian Meng, Mingpeng Li, Guanyu Lu, Zichao Shen, Simin Wu, Huazhe Liang, Zhixiang Li, Guanghao Lu, Zhaoyang Yao, Chenxi Li, Xiangjian Wan,\* and Yongsheng Chen\*

Molecule engineering has been demonstrated as a valid strategy to adjust the active layer morphology in all-small-molecule organic solar cells (ASM-OSCs). In this work, two non-fullerene acceptors (NFAs), FO-2Cl and FO-EH-2Cl, with different alkyl side chains are reported and applied in ASM-OSCs. Compared with FO-2Cl, FO-EH-2Cl is designed by replacing the octyl alkyl chains with branched *iso*-octyl alkyl chains, leading to an enhanced molecular packing, crystallinity, and redshifted absorption. With a small molecule BSFTR as donor, the device of BSFTR:FO-EH-2Cl obtains a better morphology and achieves a higher power conversion efficiency (PCE) of 15.78% with a notable fill factor (FF) of 80.44% than that of the FO-2Cl-based device with a PCE of 15.27% and FF of 78.41%. To the authors' knowledge, the FF of 80.44% is the highest value in ASM-OSCs. These results demonstrate a good example of fine-tuning the molecular structure to achieve suitable active layer morphology with promising performance for ASM-OSCs, which can provide valuable insight into material design for high-efficiency ASM-OSCs.

definite chemical structures, less batch-to-batch variation and better device performance repeatability.<sup>[1b,3]</sup> Consequently, all-small-molecule organic solar cells (ASM-OSCs) have exhibited enormous potential and achieved much progress with PCEs over 16% in recent years.<sup>[4]</sup> However, the morphology of ASM-OSCs is difficult to regulate since small molecules cannot form pre-aggregation in the solution and most of efficient small molecule donors and acceptors have the similar acceptor-donor-acceptor (A-D-A) architectures. Thus, ASM-OSCs usually output a poor fill factor (FF), lower short-circuit current ( $J_{sc}$ ) and thus low efficiencies compared with their polymer counterpart.<sup>[1e,5]</sup> Note that the  $V_{oc}$  of ASM-OSCs are comparable and even higher than their polymer counterparts. To promote the photovoltaic performance of ASM-OSCs, many efforts have

## 1. Introduction

Organic solar cells (OSCs) have attracted significant attention due to their excellent properties such as low cost, light weight, flexibility and etc.<sup>[1]</sup> Recently, power conversion efficiencies (PCEs) over 18% have been achieved for polymer-based devices with active layer material designing and device engineering.<sup>[2]</sup> However, polymer-based OSCs suffer from the batch-to-batch issue of polymers and thus the variation of device performance. In contrast, small molecules exhibit unique advantages of

been devoted to the active layer morphology manipulation via molecule design and device optimization in order to get high FF and  $J_{sc}$ .<sup>[4d,6]</sup> The molecule level optimization via the careful chemical structure design plays an indispensable and fundamental role in manipulating the morphology and have made much progress for boosting the efficiencies of ASM-OSCs. It is worth noting that more attentions have been focused on the small molecule donor design for ASM-OSCs, especially after the invention of Y6 series acceptors. However, currently, most ASM-OSCs including Y6-based devices demonstrate efficiencies below 15%.<sup>[7]</sup> Only a few cases have obtained efficiencies over 16%.<sup>[4a-c]</sup> Therefore, it is still a challenge to carefully design small molecules including donors and acceptors and regulate the active layer morphology from the molecule level optimization together with device optimization.

In our previous work, we have designed a series of A-D-A type small molecule donors and acceptors.<sup>[1b,8]</sup> Among them, the acceptors incorporating fluorene as the central unit have been systematically investigated and delivered excellent photovoltaic performance in different systems.<sup>[9]</sup> Especially, to broaden the absorption range, we designed the acceptor FO-2F by inserting oxygen atom into the molecular backbone and achieved a PCE over 15% with PM6 as donor, which is one of only a few acceptors with PCE surpassing 15% other than the Y6 derivatives.<sup>[10]</sup> Following the molecule design strategy and considering the promising device performance of F-2Cl-based

L. Meng, M. Li, S. Wu, H. Liang, Z. Li, Z. Yao, C. Li, X. Wan, Y. Chen  
State Key Laboratory and Institute of Elemento-Organic Chemistry  
Centre of Nanoscale Science and Technology and Key Laboratory of  
Functional Polymer Materials  
College of Chemistry  
Nankai University  
Tianjin 300071, P. R. China  
E-mail: xjwan@nankai.edu.cn; yschen99@nankai.edu.cn  
G. Lu, Z. Shen, G. Lu  
Frontier Institute of Science and Technology  
Xi'an Jiaotong University  
Xi'an 710054, P. R. China

 The ORCID identification number(s) for the author(s) of this article can be found under <https://doi.org/10.1002/smll.202201400>.

DOI: 10.1002/smll.202201400

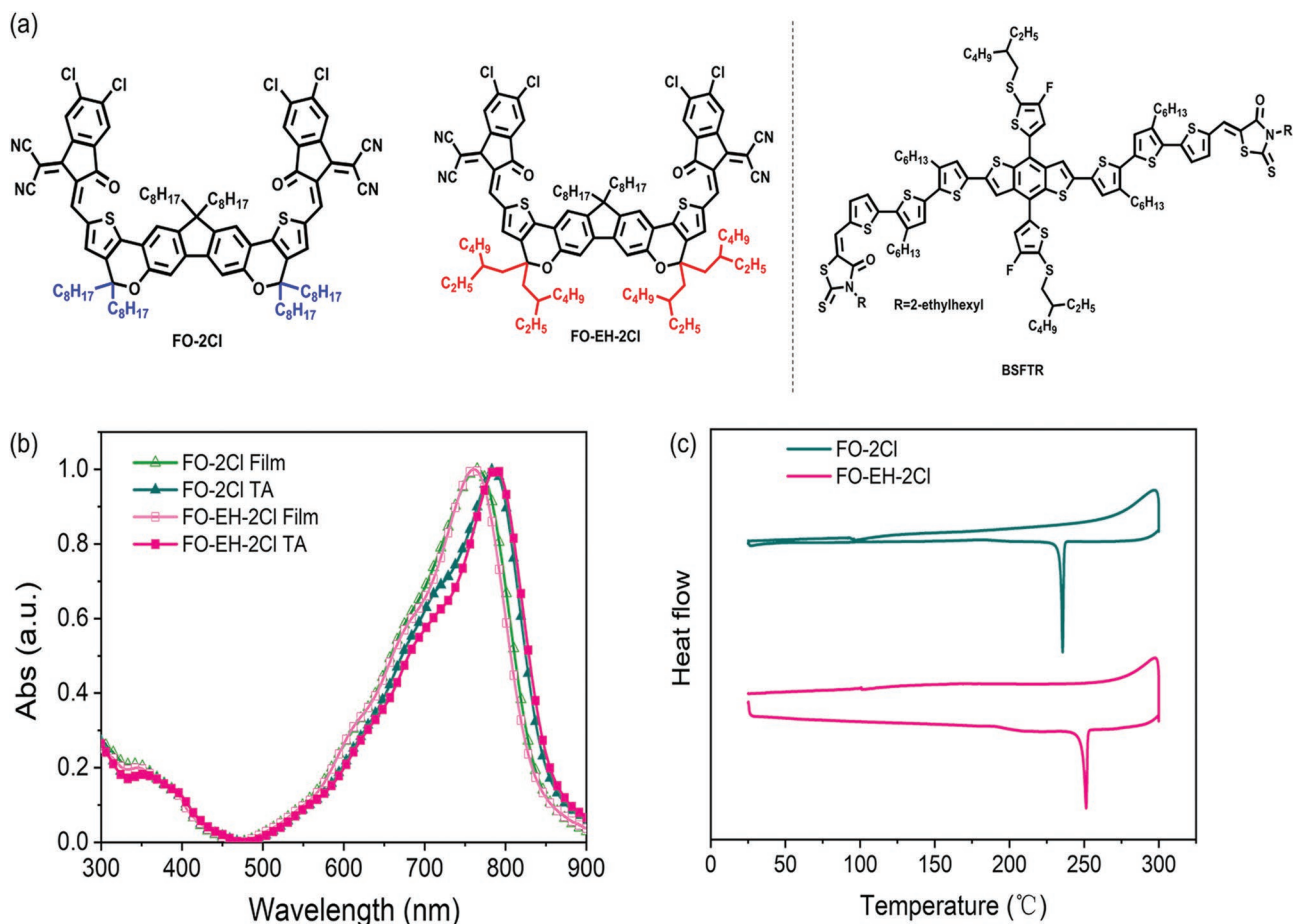


**Figure 1.** a) Chemical structures of the small molecule acceptors and donor. b) Normalized UV–vis absorption spectra in neat films for FO-2Cl and FO-EH-2Cl. c) The second cycle of DSC heating curves for FO-2Cl and FO-EH-2Cl.

ASM-OSC,<sup>[11]</sup> the acceptor FO-2Cl was designed and demonstrated a PCE of 13.91% for ASM-OSC with a small molecule C8-C-F as donor.<sup>[12]</sup> Inspired by the success of FO-2F and FO-2Cl, herein, we design and synthesize an acceptor FO-EH-2Cl by replacing the octyl alkyl chains with the branched *iso*-octyl alkyl chains to subtly modulate the active layer morphology (Figure 1a). With a small molecule donor BSFTR,<sup>[13]</sup> the two ASM-OSCs based on FO-2Cl and FO-EH-2Cl showed high PCEs of 15.27% and 15.78% with *FF* of 78.41% and 80.44%, respectively. To our knowledge, the *FF* of 80.44% is the highest value in ASM-OSCs. The notable *FF* of FO-EH-2Cl-based device is ascribed to the proper phase separation, highly efficient exciton dissociation, better carrier mobility and less bimolecular recombination.

## 2. Results and Discussion

The synthetic route of FO-EH-2Cl and the detailed characterization data are provided in the Supporting Information. Figure 1b and Figure S1 (Supporting Information) displayed the UV–vis absorption spectra of the two acceptors and the detailed data are summarized in Table 1. In dilute CHCl<sub>3</sub> solution, the two acceptors showed almost identical absorptions and similar extinction coefficient as depicted in Table 1. From the solution to solid film, the absorptions of FO-2Cl and FO-EH-2Cl depicted clearly redshifted absorptions with the maximum absorption peaks ( $\lambda_{\max}$ ) located at 765 and 761 nm, respectively, indicating the formation of dense aggregation. Moreover, with thermal annealing (TA) treatment, the  $\lambda_{\max}$  of the FO-EH-2Cl

**Table 1.** The optical and electrochemical data of FO-2Cl and FO-EH-2Cl.

Comp.	$\lambda_{\max}^{\text{sol}}$ [nm]	$\epsilon_{\max}$ [ $10^5 \text{ M}^{-1} \text{ cm}^{-1}$ ]	$\lambda_{\max}^{\text{film}}$ [nm]	$\lambda_{\text{edge}}^{\text{a)}$ [nm]	HOMO <sup>film</sup> [eV]	LUMO <sup>film</sup> [eV]
FO-2Cl	709	2.11	765 (786) <sup>b)</sup>	849 (854)	−5.83	−3.90
FO-EH-2Cl	718	2.23	761 (788)	846 (863)	−5.73	−3.90

<sup>a)</sup>Absorption onset of the molecule films; <sup>b)</sup>The values in parentheses are the absorption data with TA treatment with 135° for 5 min.

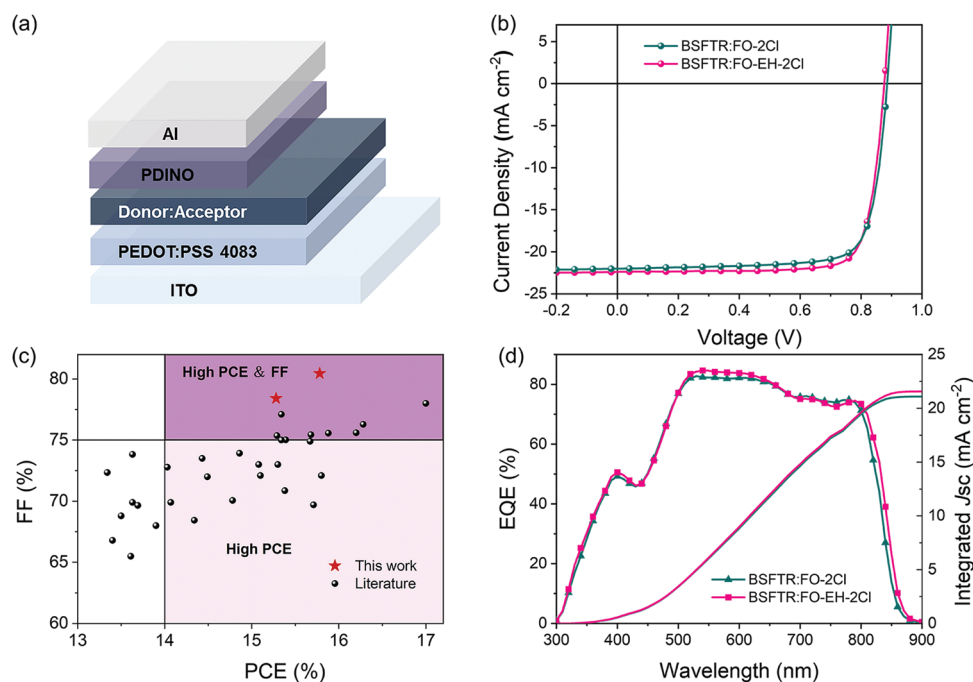


**Figure 2.** a) The device architecture of the ASM-OSC. b)  $J$ - $V$  curves of optimized devices under AM 1.5 G  $100 \text{ mW cm}^{-2}$ . c) Summary of the  $FF$  of ASM-OSCs reported in literatures with PCEs over 13% and this work. d) EQE curves and integrated photocurrent from the EQE of the optimized devices.

film is redshifted by 27 nm with the absorption onset ( $\lambda_{\text{onset}}$ ) of 863 nm and the FO-2Cl film also displays a redshifted ( $\sim 21$  nm) behavior with the  $\lambda_{\text{onset}}$  of 854 nm, suggesting more compact packing in the FO-EH-2Cl film after thermal annealing. The thermal stability of the two acceptors was investigated by the thermogravimetric analysis (TGA) (Figure S2, Supporting Information). They all exhibited good thermal stability with 5% weight loss temperatures exceeding 300 °C. We further carried out the differential scanning calorimetry (DSC) measurements to investigate the crystallinity of the two acceptors as displayed in Figure 1c. Upon heating, the FO-2Cl shows a melting temperature ( $T_m$ ) at 235.61 °C with an enthalpy change ( $\Delta H_m$ ) of 21.31 J g<sup>-1</sup>. In contrast, the  $T_m$  of the FO-EH-2Cl is much higher at 251.36 °C with a  $\Delta H_m$  of 24.92 J g<sup>-1</sup>, suggesting much better molecule packing and stronger crystallinity of FO-EH-2Cl. Cyclic voltammetry (CV) measurements were carried out to investigate the electrochemical properties of the two acceptors (Figure S3, Supporting Information), and the calculated highest occupied molecular orbital (HOMO) and lowest unoccupied molecular orbital (LUMO) energy levels are listed in Table 1. From the CV curves, the HOMO and LUMO energy levels of FO-2Cl and FO-EH-2Cl were estimated to be  $-5.83/-3.90$  eV and  $-5.73/-3.90$  eV, respectively. The two acceptors showed the same LUMO values owing to the same end groups. The slightly difference of HOMO levels should originate from the packing difference of the two acceptors.

ASM-OSCs with the conventional structure of indium tin oxide (ITO)/poly(3,4-ethylenedioxythiophene):poly(styrenesulfonate) (PEDOT:PSS)/Active Layer/perylene diimide functionalized with amino N-oxide (PDINO)/Al (Figure 2a) were fabricated to investigate the photovoltaic performance of the two acceptors, where a wide bandgap small molecule donor BSFTR

was selected as the donor.<sup>[13]</sup> The current density-voltage ( $J$ - $V$ ) characteristic curves of the two optimized ASM-OSCs were depicted in Figure 2b, and the detailed photovoltaic parameters were listed in Table 2. After TA treatment at 135 °C for 5 min for the active layers, the optimized device based on BSFTR:FO-2Cl delivered a PCE of 15.27% with a  $V_{\text{oc}}$  of 0.885 V, a  $J_{\text{sc}}$  of 22.01 mA cm<sup>-2</sup> and a notable  $FF$  of 78.41%. In contrast, the device based on BSFTR:FO-EH-2Cl achieved a PCE of 15.78% with a  $V_{\text{oc}}$  of 0.876 V, a  $J_{\text{sc}}$  of 22.39 mA cm<sup>-2</sup> and an outstanding  $FF$  of 80.44% (details in Table S1-S5 in the Supporting Information). Figure 2c and Table S6 summarized the  $FF$  versus PCE values of high efficiency ASM-OSCs reported in the literatures and this work. The  $FF$  of 80.44% is the highest value for ASM-OSCs reported to date and among the only several cases for all OSCs with  $FF$  over 80%.<sup>[2b,e,14]</sup> The results highlight the potential of ASM-OSCs, i.e., definitely comparable and/or even higher photovoltaic parameters and thus efficiencies can be obtained for ASM-OSCs compared with polymer based OSCs.

The external quantum efficiency (EQE) curves of the optimal devices based on BSFTR:FO-2Cl and BSFTR:FO-EH-2Cl are shown in Figure 2d. The two devices show similar broad

**Table 2.** The optimized photovoltaic parameters of FO-2Cl- and FO-EH-2Cl-based devices under the illumination of AM 1.5G ( $100 \text{ mW cm}^{-2}$ ).

Active layer	$V_{\text{oc}}$ [V]	$FF$ [%]	$J_{\text{sc}}$ [mA cm <sup>-2</sup> ]	$J_{\text{sc}}^{\text{EQE}}$ [mA cm <sup>-2</sup> ]	PCE [%] <sup>a)</sup>
BSFTR:FO-2Cl	0.885	78.41	22.01	21.40	15.27 (15.08)
BSFTR:FO-EH-2Cl	0.876	80.44	22.39	21.88	15.78 (15.57)

<sup>a)</sup>The average values in parentheses are obtained from 10 independent cells.

photo-response in the range of 300–880 nm. The integral current densities from the EQE curves of the devices based on FO-2Cl and FO-EH-2Cl are 21.40 and 21.88 mA cm<sup>-2</sup>, respectively, which are consistent with the  $J_{sc}$  values from  $J$ - $V$  measurements.

The energy loss ( $E_{loss}$ ) analysis of the two ASM-OSCs were conducted according to the literature method.<sup>[15]</sup> The  $E_{loss}$  of the two devices were calculated using the equation  $E_{loss} = E_{gap} - qV_{oc}$ , where the  $E_{gap}$  was estimated by the intersections between the absorption and emission spectra of the low bandgap component (Figure S4, Supporting Information). As summary in Table S7, the two ASM-OSCs of BSFTR:FO-2Cl and BSFTR:FO-EH-2Cl showed  $E_{loss}$  of 0.638 and 0.639 eV, respectively. The relatively large  $E_{loss}$  values were mainly attributed to the big non-radiative recombination loss  $\Delta E_3$  with values of 0.274 and 0.278 eV for the FO-2Cl- and FO-EH-2Cl- based devices, indicating that there are still much enhanced room for the molecule design and device optimization.

In order to investigate the exciton dissociation and charge extraction processes, the dependence of photocurrent density ( $J_{ph}$ ) versus the effective voltage ( $V_{eff}$ ) of these two devices was measured (Figure 3a).  $J_{ph}$  is defined as  $J_{ph} = J_L - J_D$ , where  $J_L$  and  $J_D$  represent the photocurrent density under illumination and dark conditions, respectively. The effective voltage  $V_{eff}$  is defined as  $V_{eff} = V_0 - V_{bias}$ , where  $V_0$  is the voltage at which  $J_{ph}$  is zero and  $V_{bias}$  is the applied external voltage bias. The value of  $P_{diss}$  calculated from  $J_{ph}$  under the short-circuit condition divided by the saturated photocurrent density ( $J_{sat}$ ), were 98.21% and 98.29% for FO-2Cl and FO-EH-2Cl-based devices, respectively, demonstrating highly efficient exciton dissociation

for the two devices. The charge separation behavior was also characterized by photoluminescence (PL) spectra. As shown in Figure S5 in the Supporting Information, the two systems lead to efficient quenching of the two blend films, suggesting that the ultra-fast charge transfer occurred between the donor and acceptors. Besides, the recombination mechanism in devices was studied by measuring the dependence of  $J_{sc}$  on light intensity ( $P_{light}$ ). Generally, the relationship is described as  $J_{sc} \propto P_{light}^\alpha$ , where  $\alpha$  is a factor related to bimolecular recombination. The devices show rather weak bimolecular recombination behavior if the  $\alpha$  value close to 1. As shown in Figure 3b, the  $\alpha$  of the devices based on BSFTR:FO-2Cl and BSFTR:FO-EH-2Cl are 0.987 and 0.991, respectively, implying that both of the devices show weak bimolecular recombination behavior.

To further investigate the charge carrier dynamics of the two devices, the transient photovoltage and photocurrent (TPV and TPC) measurements were carried out. As shown in Figure 3c, FO-EH-2Cl-based device showed a sweepout time of 0.11  $\mu$ s, much shorter than the FO-2Cl-based device (0.21  $\mu$ s), indicating that the BSFTR:FO-EH-2Cl device could effectively facilitate charge carrier extraction. Figure 3d revealed the TPV measurement of the two devices, the carrier lifetimes were 25.2  $\mu$ s and 32.9  $\mu$ s for FO-2Cl- and FO-EH-2Cl-based device, respectively. The longer carrier lifetime of FO-EH-2Cl-based device supported its weaker recombination and higher FF.<sup>[14a]</sup>

The space-charge-limited current (SCLC) method was employed to gain more insight of the properties of carrier transport. As shown in Figure S6 and Table S8 in the Supporting Information, the electron/hole mobilities were calculated to be

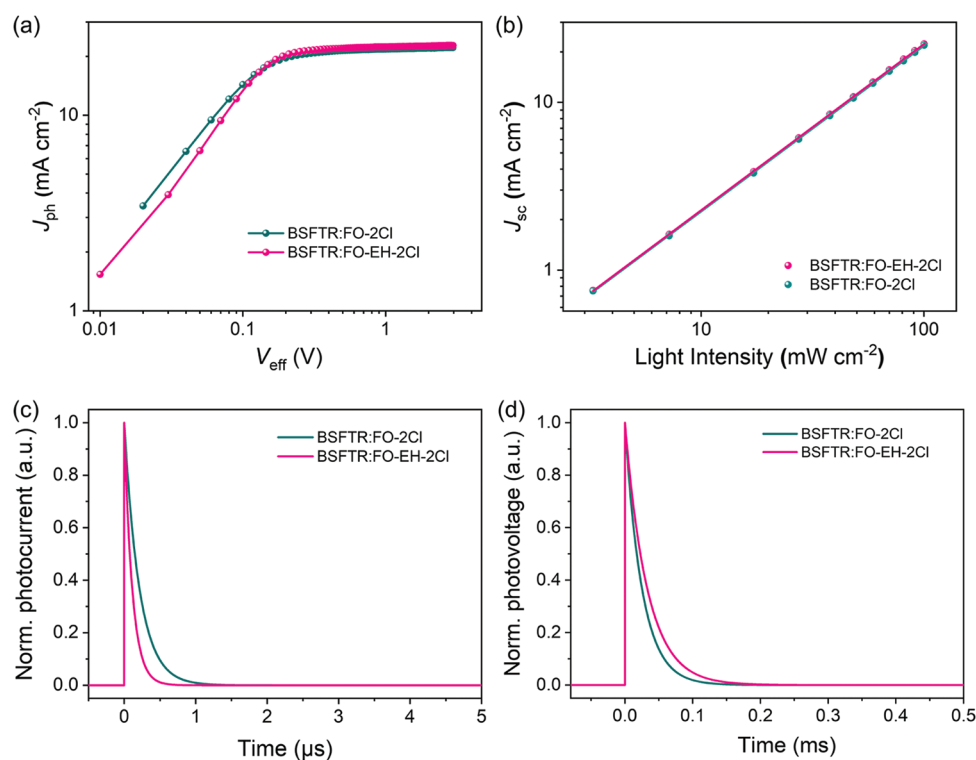


**Figure 3.** a)  $J_{ph}$  versus  $V_{eff}$ , b) Light intensity ( $P$ ) dependence of  $J_{sc}$ , c) transient photocurrent measurements and d) transient photovoltage measurements of optimized BSFTR:FO-2Cl- and BSFTR:FO-EH-2Cl-based devices.

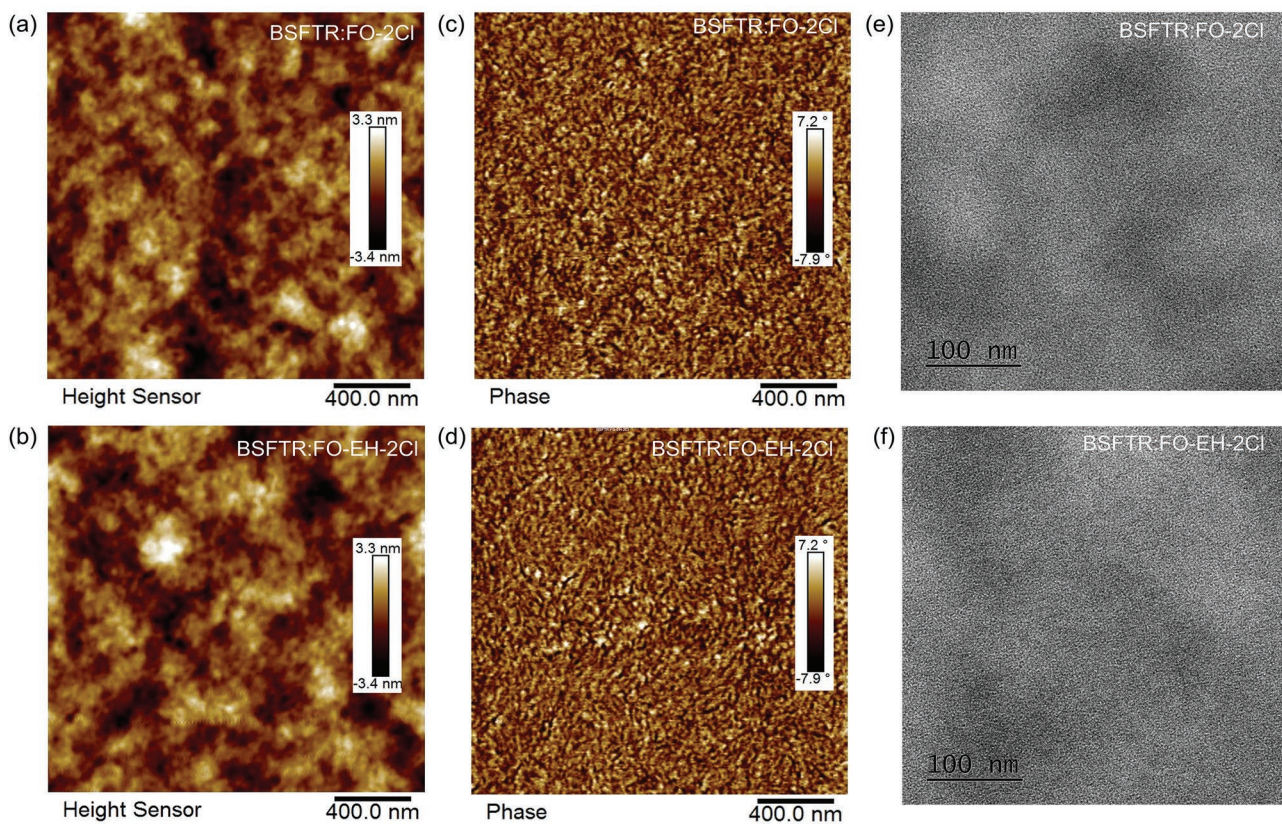


**Figure 4.** AFM height images of a) BSFTR:FO-2Cl blend and b) BSFTR:FO-EH-2Cl blend. AFM phase images of c) BSFTR:FO-2Cl blend and d) BSFTR:FO-EH-2Cl blend. TEM images of e) BSFTR:FO-2Cl blend and f) BSFTR:FO-EH-2Cl blend.

$4.13 \times 10^{-4}/2.21 \times 10^{-4} \text{ cm}^2 \text{ V}^{-1} \text{ s}^{-1}$  and  $4.64 \times 10^{-4}/3.48 \times 10^{-4} \text{ cm}^2 \text{ V}^{-1} \text{ s}^{-1}$  for the blend films of BSFTR:FO-2Cl and BSFTR:FO-EH-2Cl, corresponding to the  $\mu_e/\mu_h$  values of 1.87 and 1.33 respectively. The high mobility and balanced  $\mu_e/\mu_h$  in the blend film of BSFTR:FO-EH-2Cl was beneficial to suppress the charge accumulation and recombination and favorable for the charge transport, which enables the higher *FF* for the photovoltaic device.

Atomic force microscopy (AFM) and transmission electron microscopy (TEM) measurements were conducted to investigate the active layer morphologies of the two devices. As shown in **Figure 4a,b**, the blend films of BSFTR:FO-2Cl and BSFTR:FO-EH-2Cl both showed smooth surfaces morphology with the root-mean-square roughness ( $R_q$ ) values of 0.91 and 0.96 nm, respectively. As depicted in the AFM phase images (**Figure 4c,d**) and TEM images (**Figure 4e,f**), there exist interpenetrating structure with small fibers for the two blend films, which is favorable for the charge dissociation and transport and endows high *FF* of the corresponding devices.

To further study the morphological characteristics of the active layer, the grazing-incidence wide-angle X-ray scattering (GIWAXS) was employed to investigate the molecular packing motifs. **Figure S7** in the Supporting Information depicted the two-dimensional (2D) diffraction images and the corresponding 1D plots of in the in-plane (IP) and out-of-plane (OOP) direction of the two acceptors. As can be seen, both the neat films show strong  $\pi$ - $\pi$  stacking diffraction peaks (010) in OOP direction and lamellar packing diffraction (100) in IP direction,

corresponding to predominant face-on orientation. Additionally, FO-EH-2Cl displayed the same  $\pi$ - $\pi$  stacking distance of 3.57 Å in the OOP direction with FO-2Cl, but a larger crystal coherence length (CCL) of 64.98 Å than FO-2Cl (61.78 Å), demonstrating the more ordered packing and higher crystallinity.<sup>[4b,16]</sup> The donor material BSFTR shows a preferential edge-on orientation as previous reported.<sup>[13]</sup> Upon mixing with the BSFTR, the GIWAXS images of the blend films for BSFTR:FO-2Cl and BSFTR:FO-EH-2Cl as displayed in **Figure 5a–c** and **Table S9**. Both blend films tend to form mixed face-on and edge-on packing modes with the 3D network, which could facilitate charge transport.<sup>[5d,16]</sup> In the OOP direction, the blend for BSFTR:FO-EH-2Cl shows an approximate  $\pi$ - $\pi$  stacking distances with BSFTR:FO-2Cl (3.64 Å for the FO-2Cl-based blend and 3.65 Å for the FO-EH-2Cl based blend) and a slightly smaller CCL value of 59.02 Å compared with FO-2Cl (65.35 Å). However, in the IP direction, the  $\pi$ - $\pi$  stacking distances for FO-2Cl- and FO-EH-2Cl-based blend film are 3.66 Å and 3.64 Å, with CCL values of 29.57 Å and 67.93 Å, respectively. Obviously, FO-EH-2Cl-based blend film shows a smaller  $\pi$ - $\pi$  stacking distances and rather larger CCL value than FO-2Cl-based blend film, indicating a more closely and ordered packing. Unlike the FO-2Cl-based blend with a relatively poor packing ability in the IP direction, FO-EH-2Cl-based blend show good packing ability in both IP and OOP directions, which is beneficial for charge transport and account for the high mobility, weaker recombination and thus superior *FF*.

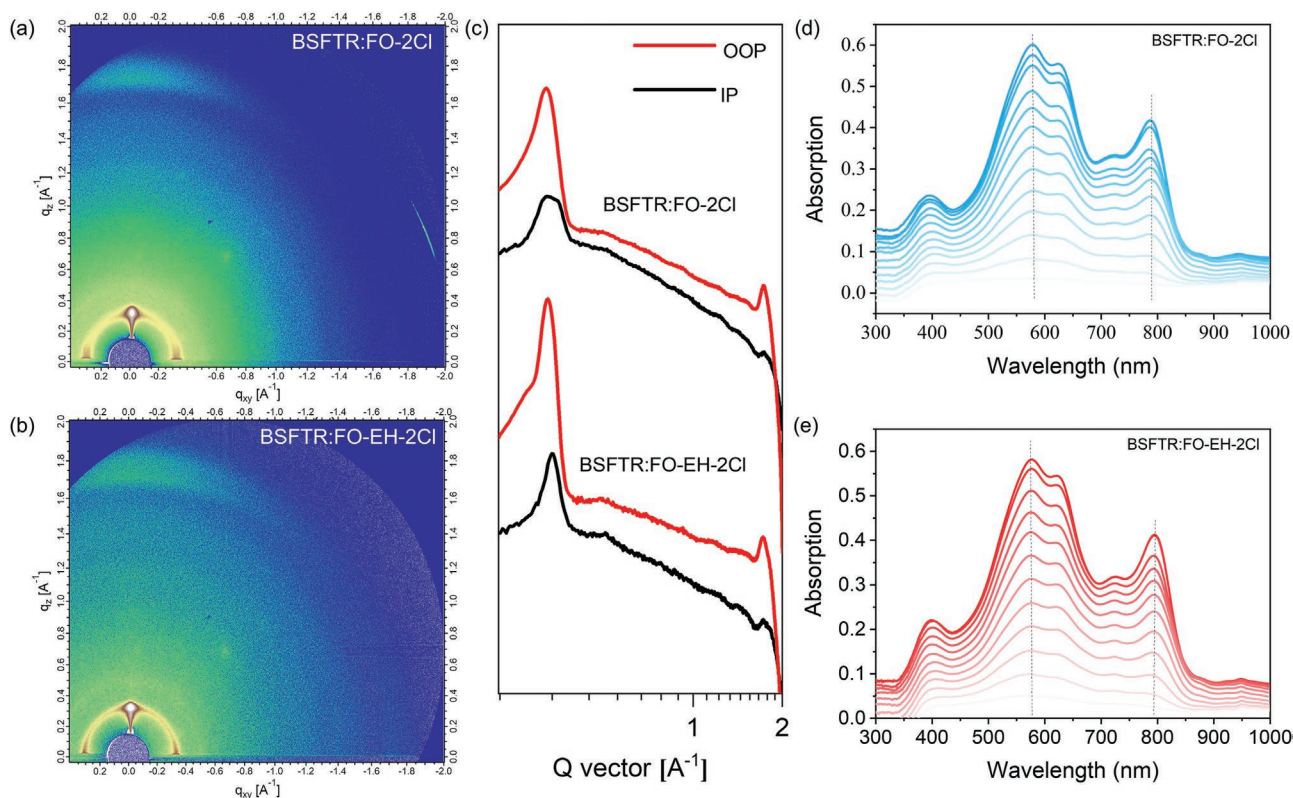


**Figure 5.** 2D-GIWAXD diffraction images of a) BSFTR:FO-2Cl blend and b) BSFTR:FO-EH-2Cl blend; c) 1D plots of the blend films in the in-plane and out of plane direction; Film-depth-dependent absorption spectra of d) BSFTR:FO-2Cl blend and e) BSFTR:FO-EH-2Cl blend.

We further conducted the contact angle and film-depth dependent light absorption spectroscopy (FLAS) measurements to study the vertical phase separation and figure out the miscibility between BSFTR and acceptors. The interaction between the donor and acceptor materials is an essential estimated index for miscibility of the blend film and usually confirmed by the Flory–Huggins interaction parameter  $\chi_{\text{donor,acceptor}}$  which can be obtained from the empirical equation of  $\chi = K(\sqrt{\gamma_{\text{donor}}} - \sqrt{\gamma_{\text{acceptor}}})^2$ , where  $K$  is a constant,  $\gamma_{\text{donor}}$  and  $\gamma_{\text{acceptor}}$  represent the surface tensions of the donor and acceptor materials.<sup>[17]</sup> According to the contact angle data for the donor and acceptors, the  $\gamma$  can be calculated by Owens-Wendt-Kaelble's model.<sup>[18]</sup> As shown in Table S10, we find that by employing the branched alky side chains to the acceptor, the calculated  $\chi$  value increases from 0.17  $K$  for the FO-2Cl-based blend to 0.23  $K$  for the FO-EH-2Cl-based, indicating a lower miscibility in the BSFTR:FO-EH-2Cl blend film. The alleviated miscibility of BSFTR:FO-EH-2Cl is favor of suitable phase separation and realize efficient charge transport at the D:A interface and benefit to higher  $FF$  and  $J_{\text{sc}}$ ,<sup>[16,19]</sup> supporting the SCLC, TEM and AFM results.

Additionally, the FLAS measurements were also carried out to semi-empirically figure out the kinetically vertically-resolved miscibility and vertical phase separation in the corresponding blends as shown in Figure 5d,e.<sup>[20]</sup> Here,  $\beta$  is self-defined as follows:  $\beta = \frac{\sum_1^n |a - b_i|}{n}$ , where  $a$  and  $b_i$  are the ratios of D/A absorbance at the characteristic absorption wavelength of the

whole film and sublayers,  $n$  is the numbers of the sublayers. The  $\beta$  values were 1.77 for FO-2Cl-based blend and 0.92 for FO-EH-2Cl-based blend, and according to the definition, a smaller  $\beta$  usually means the FO-EH-2Cl-based blend established a better vertical phase miscibility, indicating the homogenous vertical phase for donor and acceptor and contribute to weaken the vertical fluctuation of transport energy levels and avoid some insufficient charge transport channels at some film-depths,<sup>[21]</sup> which was beneficial for higher  $FF$  and PCE. Furthermore, the film depth-dependent composition profiles shown in Figure S8 in the Supporting Information exhibits the content of BSFTR and FO-EH-2Cl are closer to each other than the content of BSFTR and FO-2Cl, supporting above results.<sup>[20b]</sup> These results suggest that the BSFTR:FO-EH-2Cl-based device develops with a homogenous and proper vertical phase separation and better vertical miscibility, which is beneficial for charge extraction and transport and favor of its higher  $FF$  and  $J_{\text{sc}}$ .

### 3. Conclusion

In summary, we have reported two acceptors, FO-2Cl and FO-EH-2Cl with different side chains on the same molecular backbone. The ASM-OSCs based on these two acceptors all showed promising efficiencies over 15%. Especially, the device based on FO-EH-2Cl with the branched chains demonstrated a PCE of 15.78% with an outstanding  $FF$  of 80.44%. Compared with FO-2Cl, FO-EH-2Cl shows a better crystallinity, more ordered

packing mode and suitable phase separation in its blending film with the donor BSFTR, leading to more efficient charge extraction and charge transport, faster charge collection and weaker recombination. Our results suggest a facile strategy to finely tune the molecular structures for achieving suitable morphology and improving the performance of ASM-OSCs. It is strongly believed that ASM-OSCs with comparable and even higher efficiencies can be obtained via the careful molecule design and device optimization.

## Supporting Information

Supporting Information is available from the Wiley Online Library or from the author.

## Acknowledgements

L.X.M. and M.P.L. contributed equally to this work. The authors gratefully acknowledge the financial support from NSFC (52025033 and 21935007), MoST (2019YFA0705900) of China, Tianjin city (20JCZDJC00740), and 111 Project (B12015).

## Conflict of Interest

The authors declare no conflict of interest.

## Data Availability Statement

The data that support the findings of this study are available in the supplementary material of this article.

## Keywords

alkyl side chains, all-small-molecule organic solar cells, fill factor, non-fullerene acceptors

Received: March 3, 2022

Revised: March 25, 2022

Published online:

- [1] a) R. Sun, Q. Wu, J. Guo, T. Wang, Y. Wu, B. B. Qiu, Z. H. Luo, W. Y. Yang, Z. C. Hu, J. Guo, M. M. Shi, C. L. Yang, F. Huang, Y. F. Li, J. Min, *Joule* **2020**, *4*, 407; b) X. Wan, C. Li, M. Zhang, Y. Chen, *Chem. Soc. Rev.* **2020**, *49*, 2828; c) Y. Sun, M. Chang, L. Meng, X. Wan, H. Gao, Y. Zhang, K. Zhao, Z. Sun, C. Li, S. Liu, H. Wang, J. Liang, Y. Chen, *Nat. Electron.* **2019**, *2*, 513; d) Y. Sun, T. Liu, Y. Kan, K. Gao, B. Tang, Y. Li, *Small Sci.* **2021**, *1*, 2100001; e) Y. Wei, J. Yu, L. Qin, H. Chen, X. Wu, Z. Wei, X. Zhang, Z. Xiao, L. Ding, F. Gao, H. Huang, *Energy Environ. Sci.* **2021**, *14*, 2314.
- [2] a) Z. Zheng, J. Wang, P. Bi, J. Ren, Y. Wang, Y. Yang, X. Liu, S. Zhang, J. Hou, *Joule* **2022**, *6*, 171; b) K. Chong, X. Xu, H. Meng, J. Xue, L. Yu, W. Ma, Q. Peng, *Adv. Mater.* **2022**, *34*, 2109516; c) Y. Lin, M. I. Nugraha, Y. Firdaus, A. D. Scaccabarozzi, F. Aniés, A.-H. Emwas, E. Yengel, X. Zheng, J. Liu, W. Wahyudi, E. Yarali, H. Faber, O. M. Bakr, L. Tsetseris, M. Heeney, T. D. Anthopoulos, *ACS Energy Lett.* **2020**, *5*, 3663; d) K. Jin, Z. Xiao, L. Ding, *J. Semi-cond.* **2021**, *42*, 060502; e) C. Li, J. Zhou, J. Song, J. Xu, H. Zhang, X. Zhang, J. Guo, L. Zhu, D. Wei, G. Han, J. Min, Y. Zhang, Z. Xie, Y. Yi, H. Yan, F. Gao, F. Liu, Y. Sun, *Nat. Energy* **2021**, *6*, 605.
- [3] a) Y. Chen, X. Wan, G. Long, *Acc. Chem. Res.* **2013**, *46*, 2645; b) J. Hou, O. Inganas, R. H. Friend, F. Gao, *Nat. Mater.* **2018**, *17*, 119.
- [4] a) J. Qin, Z. Chen, P. Bi, Y. Yang, J. Zhang, Z. Huang, Z. Wei, C. An, H. Yao, X. Hao, T. Zhang, Y. Cui, L. Hong, C. Liu, Y. Zu, C. He, J. Hou, *Energy Environ. Sci.* **2021**, *14*, 5903; b) L. Zhang, X. Zhu, D. Deng, Z. Wang, Z. Zhang, Y. Li, J. Zhang, K. Lv, L. Liu, X. Zhang, H. Zhou, H. Ade, Z. Wei, *Adv. Mater.* **2022**, *34*, 2106316; c) M. Jiang, H. Bai, H. Zhi, L. Yan, H. Y. Woo, L. Tong, J. Wang, F. Zhang, Q. An, *Energy Environ. Sci.* **2021**, *14*, 3945; d) L. Nian, Y. Kan, K. Gao, M. Zhang, N. Li, G. Zhou, S. B. Jo, X. Shi, F. Lin, Q. Rong, F. Liu, G. Zhou, A. K. Y. Jen, *Joule* **2020**, *4*, 2223.
- [5] a) H. Chen, D. Hu, Q. Yang, J. Gao, J. Fu, K. Yang, H. He, S. Chen, Z. Kan, T. Duan, C. Yang, J. Ouyang, Z. Xiao, K. Sun, S. Lu, *Joule* **2019**, *3*, 3034; b) K. Gao, S. B. Jo, X. Shi, L. Nian, M. Zhang, Y. Kan, F. Lin, B. Kan, B. Xu, Q. Rong, L. Shui, F. Liu, X. Peng, G. Zhou, Y. Cao, A. K. Jen, *Adv. Mater.* **2019**, *31*, 1807842; c) J. Ge, L. Xie, R. Peng, B. Fanady, J. Huang, W. Song, T. Yan, W. Zhang, Z. Ge, *Angew. Chem., Int. Ed. Engl.* **2019**, *59*, 2808; d) R. Zhou, Z. Jiang, C. Yang, J. Yu, J. Feng, M. A. Adil, D. Deng, W. Zou, J. Zhang, K. Lu, W. Ma, F. Gao, Z. Wei, *Nat. Commun.* **2019**, *10*, 5393; e) D. Hu, Q. Yang, H. Chen, F. Wobben, V. M. Le Corre, R. Singh, T. Liu, R. Ma, H. Tang, L. J. A. Koster, T. Duan, H. Yan, Z. Kan, Z. Xiao, S. Lu, *Energy Environ. Sci.* **2020**, *13*, 2134; f) B. Qiu, Z. Chen, S. Qin, J. Yao, W. Huang, L. Meng, H. Zhu, Y. M. Yang, Z. G. Zhang, Y. Li, *Adv. Mater.* **2020**, *32*, 1908373.
- [6] a) Z. Zhou, S. Xu, J. Song, Y. Jin, Q. Yue, Y. Qian, F. Liu, F. Zhang, X. Zhu, *Nat. Energy* **2018**, *3*, 952; b) T. Xu, J. Lv, K. Yang, Y. He, Q. Yang, H. Chen, Q. Chen, Z. Liao, Z. Kan, T. Duan, K. Sun, J. Ouyang, S. Lu, *Energy Environ. Sci.* **2021**, *14*, 5366; c) R. Sun, Y. Wu, J. Guo, Y. Wang, F. Qin, B. Shen, D. Li, T. Wang, Y. Li, Y. Zhou, G. Lu, Y. Li, J. Min, *Energy Environ. Sci.* **2021**, *14*, 3174; d) X. Zhang, L. Qin, Y. Li, J. Yu, H. Chen, X. Gu, Y. Wei, X. Lu, F. Gao, H. Huang, *Adv. Funct. Mater.* **2022**, 2112433.
- [7] B. Kan, Y. Kan, L. Zuo, X. Shi, K. Gao, *InfoMat* **2021**, *3*, 175.
- [8] a) B. Kan, H. Feng, X. Wan, F. Liu, X. Ke, Y. Wang, Y. Wang, H. Zhang, C. Li, J. Hou, Y. Chen, *J. Am. Chem. Soc.* **2017**, *139*, 4929; b) N. Qiu, H. Zhang, X. Wan, C. Li, X. Ke, H. Feng, B. Kan, H. Zhang, Q. Zhang, Y. Lu, Y. Chen, *Adv. Mater.* **2017**, *29*, 201604964; c) H. Feng, Y. Q. Yi, X. Ke, J. Yan, Y. Zhang, X. Wan, C. Li, N. Zheng, Z. Xie, Y. Chen, *Adv. Energy Mater.* **2019**, *9*, 1803541.
- [9] a) L. Meng, Y. Zhang, X. Wan, C. Li, X. Zhang, Y. Wang, X. Ke, Z. Xiao, L. Ding, R. Xia, H.-L. Yip, Y. Cao, Y. Chen, *Science* **2018**, *361*, 1094; b) Y. Wang, Y. Zhang, N. Qiu, H. Feng, H. Gao, B. Kan, Y. Ma, C. Li, X. Wan, Y. Chen, *Adv. Energy Mater.* **2018**, *8*, 1702870; c) X. Zhang, Y. Ding, H. Feng, H. Gao, X. Ke, H. Zhang, C. Li, X. Wan, Y. Chen, *Sci. China: Chem.* **2020**, *63*, 1799; d) Y. Zhang, H. Feng, L. Meng, Y. Wang, M. Chang, S. Li, Z. Guo, C. Li, N. Zheng, Z. Xie, X. Wan, Y. Chen, *Adv. Energy Mater.* **2019**, *9*, 1902688.
- [10] X. Ke, L. Meng, X. Wan, M. Li, Y. Sun, Z. Guo, S. Wu, H. Zhang, C. Li, Y. Chen, *J. Mater. Chem. A* **2020**, *8*, 9726.
- [11] Y. Wang, Y. Wang, B. Kan, X. Ke, X. Wan, C. Li, Y. Chen, *Adv. Energy Mater.* **2018**, *8*, 1802021.
- [12] L. Meng, S. Wu, X. Wan, Z. Shen, M. Li, Y. Yang, J. Wang, G. Lu, Z. Ma, Z. Yao, C. Li, Y. Chen, *Chem. Mater.* **2022**, *34*, 3168.
- [13] H. Wu, Q. Yue, Z. Zhou, S. Chen, D. Zhang, S. Xu, H. Zhou, C. Yang, H. Fan, X. Zhu, *J. Mater. Chem. A* **2019**, *7*, 15944.
- [14] a) X. Zhang, C. Li, J. Xu, R. Wang, J. Song, H. Zhang, Y. Li, Y.-N. Jing, S. Li, G. Wu, J. Zhou, X. Li, Y. Zhang, X. Li, J. Zhang, C. Zhang, H. Zhou, Y. Sun, Y. Zhang, *Joule* **2022**, *6*, 444; b) Y. Zeng, D. Li, H. Wu, Z. Chen, S. Leng, T. Hao, S. Xiong, Q. Xue, Z. Ma, H. Zhu, Q. Bao, *Adv. Funct. Mater.* **2021**, *32*, 2110743; c) Z. Yihan,

- L. Danqin, X. Zuo, W. Hongbo, C. Zeng, H. Tianyu, X. Shaobing, M. Zaifei, Z. Haiming, D. Liming, B. Qinye, *Adv. Energy Mater.* **2021**, *11*, 2101338; d) Y. Cui, Y. Xu, H. Yao, P. Bi, L. Hong, J. Zhang, Y. Zu, T. Zhang, J. Qin, J. Ren, Z. Chen, C. He, X. Hao, Z. Wei, J. Hou, *Adv. Mater.* **2021**, *33*, 2102420; e) Y. Cui, H. Yao, J. Zhang, K. Xian, T. Zhang, L. Hong, Y. Wang, Y. Xu, K. Ma, C. An, C. He, Z. Wei, F. Gao, J. Hou, *Adv. Mater.* **2020**, *32*, 1908205; f) F. Bai, J. Zhang, A. Zeng, H. Zhao, K. Duan, H. Yu, K. Cheng, G. Chai, Y. Chen, J. Liang, W. Ma, H. Yan, *Joule* **2021**, *5*, 1231.
- [15] J. Yao, T. Kirchartz, M. S. Vezie, M. A. Faist, W. Gong, Z. He, H. Wu, J. Troughton, T. Watson, D. Bryant, J. Nelson, *Phys. Rev. Appl.* **2015**, *4*, 014020.
- [16] T. Duan, Q. Chen, Q. Yang, D. Hu, G. Cai, X. Lu, J. Lv, H. Song, C. Zhong, F. Liu, D. Yu, S. Lu, *J. Mater. Chem. A* **2022**, *10*, 3009.
- [17] M. A. Adil, J. Zhang, Y. Wang, J. Yu, C. Yang, G. Lu, Z. Wei, *Nano Energy* **2020**, *68*, 104271.
- [18] J. Comyn, *Int. J. Adhes. Adhes.* **1992**, *12*, 145.
- [19] a) Y. Zhao, X. Tang, J. Cao, P. Huang, C. Weng, P. Shen, *Org. Electron.* **2022**, *102*, 106446; b) B. Zheng, J. Ni, S. Li, Y. Yue, J. Wang, J. Zhang, Y. Li, L. Huo, *Adv. Sci.* **2022**, *9*, 2105430.
- [20] a) R. Sun, T. Wang, Y. Wu, M. Zhang, Y. Ma, Z. Xiao, G. Lu, L. Ding, Q. Zheng, C. J. Brabec, Y. Li, J. Min, *Adv. Funct. Mater.* **2021**, *31*, 2106846; b) S. He, Z. Shen, J. Yu, H. Guan, G. Lu, T. Xiao, S. Yang, Y. Zou, L. Bu, *Adv. Mater. Interfaces* **2020**, *7*, 2000577; c) Y. Zhang, D. Deng, Z. Wang, Y. Wang, J. Zhang, J. Fang, Y. Yang, G. Lu, W. Ma, Z. Wei, *Adv. Energy Mater.* **2017**, *7*, 1701548.
- [21] Y. Huo, X.-T. Gong, T.-K. Lau, T. Xiao, C. Yan, X. Lu, G. Lu, X. Zhan, H.-L. Zhang, *Chem. Mater.* **2018**, *30*, 8661.